Supporting Information: Vesicle dynamics in large amplitude oscillatory extension

Charlie Lin[1], Dinesh Kumar[2,3], Channing M. Richter[2], Shiyan Wang[1], Charles M. Schroeder[2,3,4], and Vivek Narsimhan[1]

[1]Davidson School of Chemical Engineering, Purdue University, West Lafayette, IN 47907
[2]Department of Chemical and Biomolecular Engineering, University of Illinois at Urbana-Champaign, Urbana, IL, 61801
[3]Beckman Institute for Advanced Science and Technology, University of Illinois at Urbana-Champaign, Urbana, IL, 61801
[4]Department of Materials Science and Engineering, University of Illinois at Urbana-Champaign, Urbana, IL, 61801

October 19, 2021

1 Experiments

1.1 Characteristic response time for actuating fluid flow in the microfluidic device

The minimum value of cycle period T in large amplitude oscillatory extension (LAOE) experiments is limited by how quickly we can actuate fluid flow in the microfluidic device. For this reason, we characterized the response time of flow turn-on and turn-off for the Elveflow pressure regulators. Fig. S1a shows the characteristic rise time and settling time for an extreme change in pressure from 0 to 4 psi during a typical experiment. Here, the time required for measured pressure to reach ∼95% of its set value is defined as rise time, and the time required for the measured pressure to settle around the set value is defined as the settling time. Clearly, the rise time for an extreme increase in pressure from 0 to 4 psi (strain rate jump from 0 to ∼30 s^{-1}) is ∼20 ms and the settling time is ∼300 ms. For all the experiments in this manuscript, we chose the lowest cycle time T to be 2 second which is much larger than the characteristic response time of fluid flow. In addition, the largest value of pressure used in experiments is 0.4 psi for which we expect lower response time.

We also characterized the response time of pressure regulators for an extreme pressure reduction from 10 psi to 0 psi (Fig. S1b). Clearly, the fall time is of the order of ∼50 ms which is much faster than the minimum cycle time period used in our experiments.

1.2 Wrinkling dynamics of quasi-spherical vesicles in large amplitude oscillatory extension

As mentioned in the main text, quasi-spherical vesicles undergo a transient wrinkling instability during the compression phase of LAOE cycle. Such wrinkling features are similar to those observed by Turitsyn & Vergeles (2008) in a single step reversal of elongational flow. In Fig. S2, Fig. S3, Fig. S4 and Fig. S5, we show two scenarios of vesicle undergoing wrinkling instability with their corresponding deformation parameter plot and Lissajous curves.

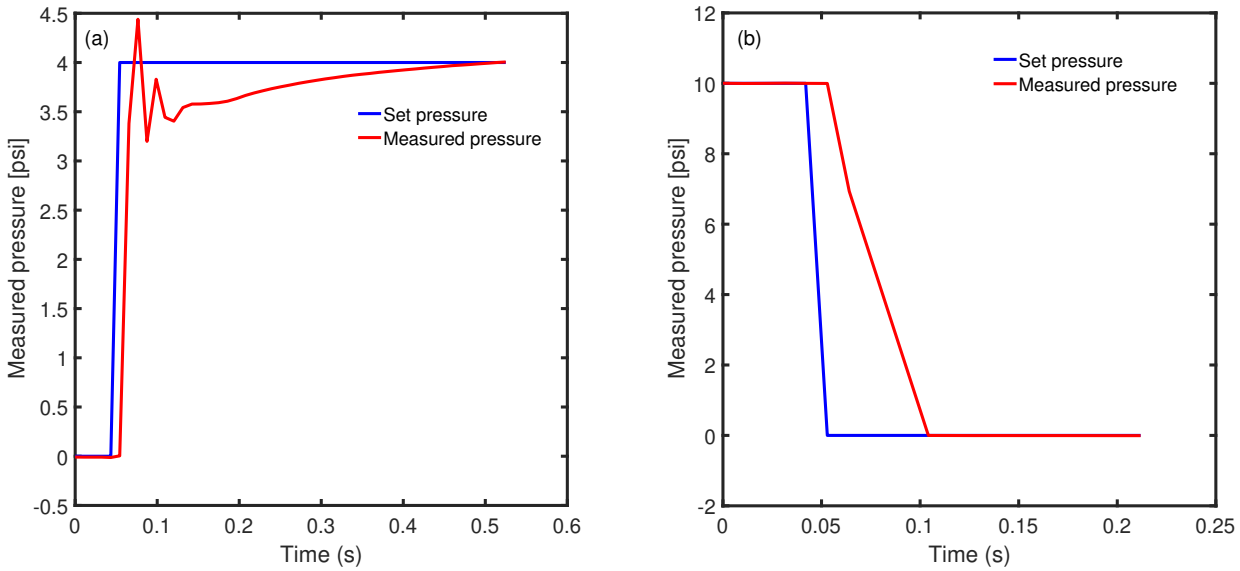

Figure 1: FIG. S1: (a) Response time of fluid flow actuation in the microfluidic device for a step increase in pressure from 0 to 4 psi. (b) Response time of fluid flow actuation in the microfluidic device for a step decrease in pressure from 10 to 0 psi

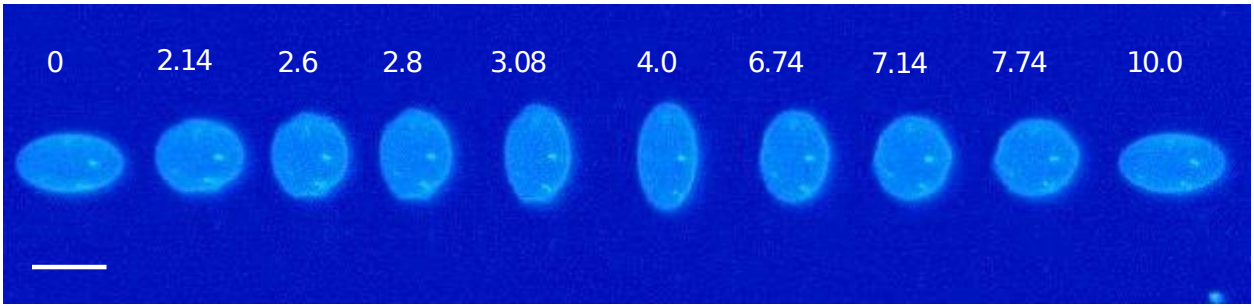

FIG. S2: Snapshots of vesicle dynamics showing wrinkling instability in large amplitude oscillatory extensional flow at reduced volume ν =0.91, flow cycle period T=10 s, Ca=344.4, and De=45.4. Scale bar is 10 μm and numbers denote time in seconds.

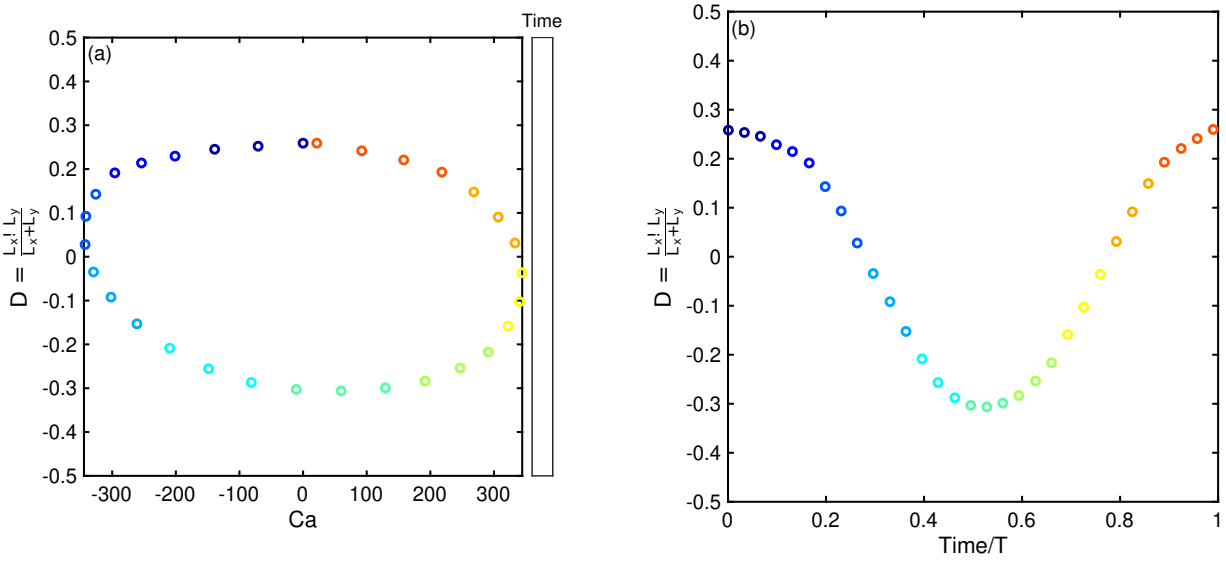

FIG. S3: LAOE deformation dynamics for the vesicle shown in Fig. S2. (a) Experimental Lissajous plot showing the deformation paramater as a function of capillary number at Ca = 344.4 and De = 45.4. The color scale denotes the time in seconds. (b) Deformation parameter as a function of time over one LAOE cycle deformation.

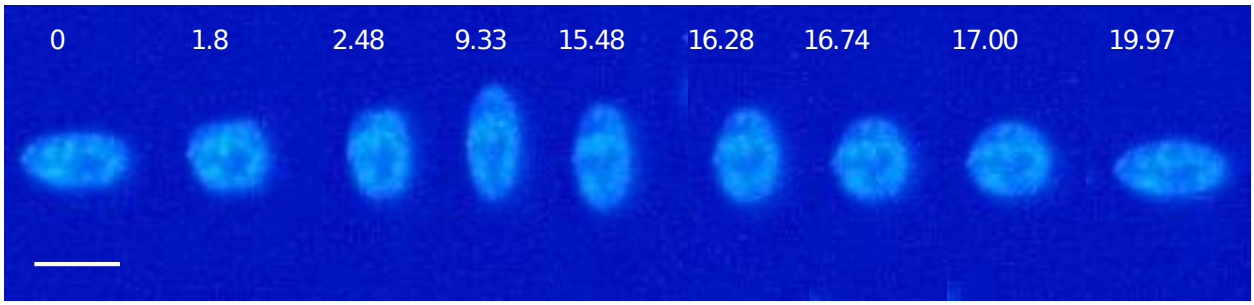

FIG. S4: Snapshots of vesicle dynamics showing wrinkling instability in large amplitude oscillatory extensional flow at reduced volume ν =0.87, flow cycle period T=30 s, Ca=351.8, and De=5.2. Scale bar is 10 μm and numbers denote time in seconds.

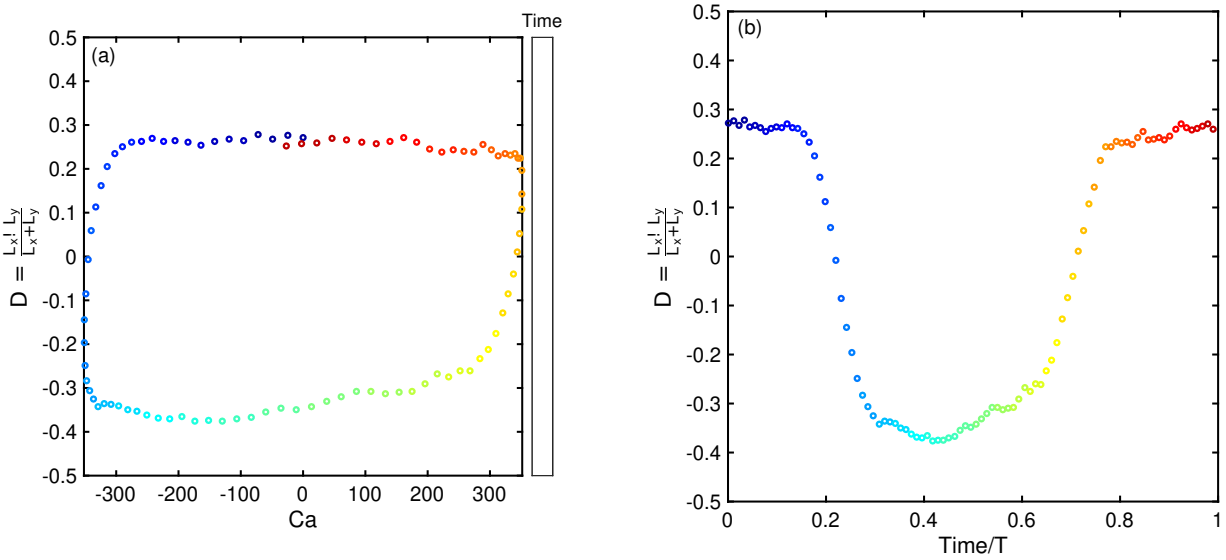

FIG. S5: LAOE deformation dynamics for the vesicle shown in Fig. S4. (a) Experimental Lissajous plot showing the deformation parameter as a function of capillary number at Ca = 351.8 and De = 5.2. The color scale denotes the time in seconds. (b) Deformation parameter as a function of time over one LAOE cycle deformation.

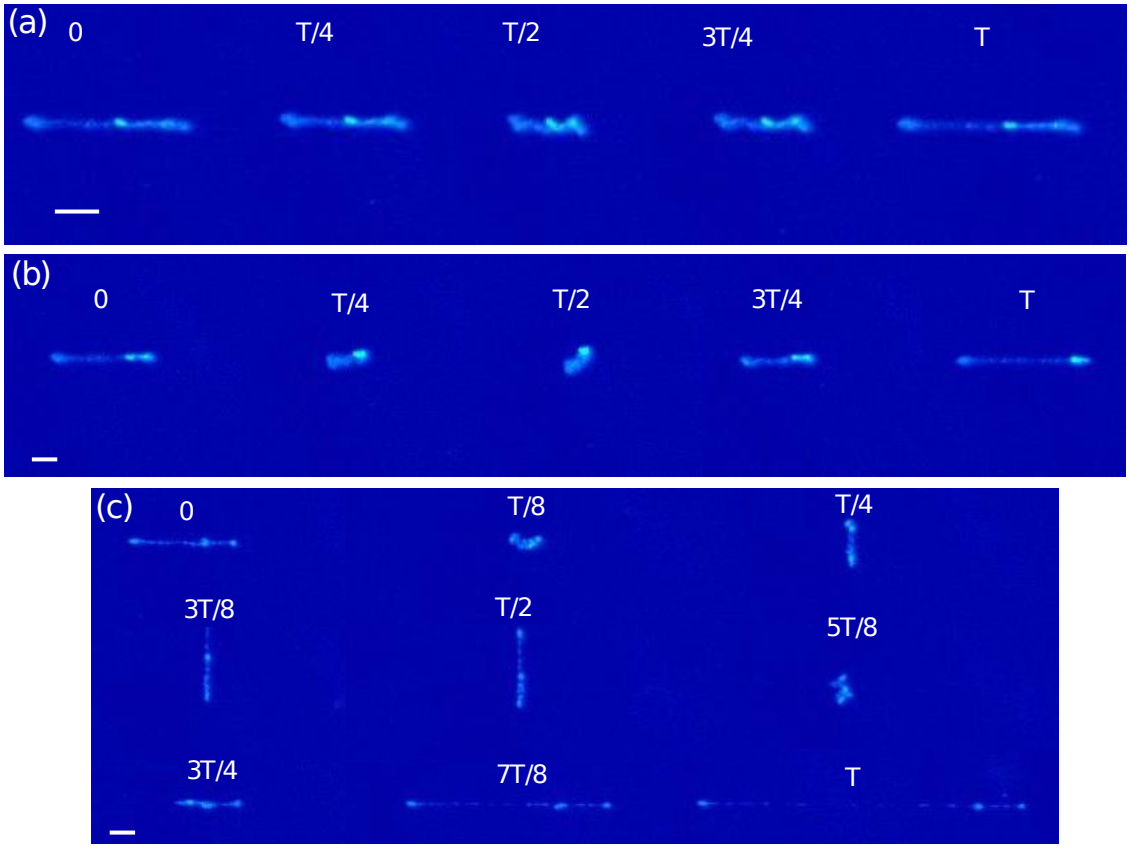

FIG. S6: Experimental snapshots of vesicle shapes over one LAOE flow cycle for the pulsating, reorienting and full reorientation regime. The values in the figure denote the fraction of cycle time. Vesicle parameters are: (a) $\nu = 0.35$, $T = 10$s, Ca $= 44.9$, De $= 5.7$, (b) $\nu = 0.35$, $T = 20$s, Ca $= 44.9$, De $= 2.9$, (c) $\nu = 0.35$, $T = 80$s, Ca $= 44.9$, De $= 0.7$. Scale bar is 10 μm.

1.3 Buckling dynamics of tubular vesicles in large amplitude oscillatory extension

In this section, we present the transient dynamics of a highly deflated vesicle ($\nu = 0.35 \pm 0.02$) in large amplitude oscillatory extension (Fig. S6). For such highly deflated vesicles, the dominant deformation occurs along the vesicle long axis and hence, it is more suitable to define the deformation parameter as L/L_0 where L is the time-dependent end-to-end length of vesicle and L_0 is the length at the beginning of flow cycle. Similar to quasi-spherical vesicles, we observe three dynamics regimes namely the pulsating (Fig. S6a), reorienting (Fig. S6b) and the full reorientation regime depending on the values of Ca and De. In the pulsating regime, the vesicle remains along the $x-$axis during the entire flow cycle as the flow frequency is very fast (Fig. S6a). When the flow frequency is slightly decreased, the vesicle membrane starts reorienting along $y-$axis but does not have sufficient time to undergo a full reorientation (Fig. S6b). At even lower flow frequency, the vesicle undergoes full reorientation along $y-$axis (Fig. S6c). Unlike quasi-spherical vesicles, we do not observe equal deformation along x and y axis for such highly deflated vesicles. In particular, we observe that vesicle adopts a U-shaped conformation at $T/4$ during orientation and both the ends of vesicle nearly overlap. As a result of U-shaped conformation, vesicle undergoes hindered stretching at $T/2$. Interestingly, the vesicle loses the U-shaped conformation after the flow reverses and undergoes full stretching towards the end of deformation cycle. The corresponding Lissajous curve and deformation plots for the three dynamical regimes are shown in Fig. S7. From this experiment, we can conlude that highly deflated vesicles undergo much more complex dynamics in time-dependent flow due to high availability of excess area.

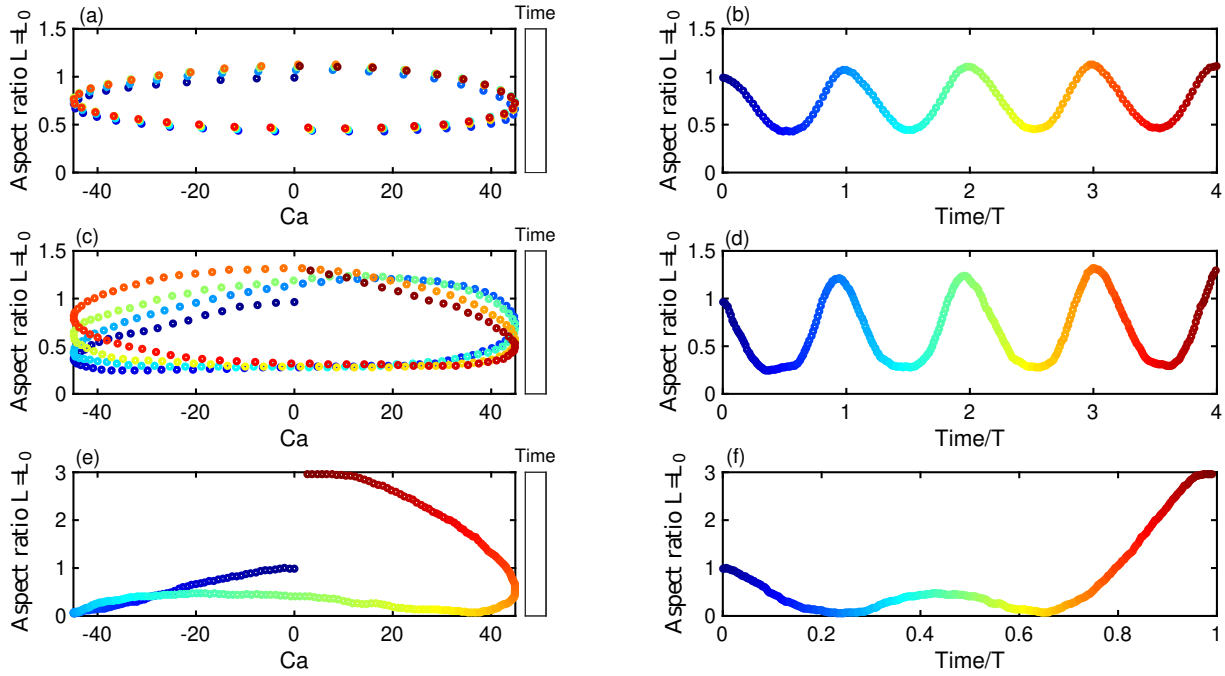

FIG. S7: Experimental single vesicle Lissajous curves and deformation plots for $\nu = 0.35$. (a,b) Lissajous-type deformation plot as a function of Ca, and deformation parameter as a function of time with time period $T = 10$ s at Ca $= 44.9$ and De $= 5.7$. The color scales denote the time t. (c,d) Lissajous-type deformation plot as a function of Ca, and deformation parameter as a function of time with time period $T = 20$ s at Ca $= 44.9$ and De $= 2.9$. (e,f) Lissajous-type deformation plot as a function of Ca, and deformation parameter as a function of time with time period $T = 80$ s at Ca $= 44.9$ and De $= 0.7$.

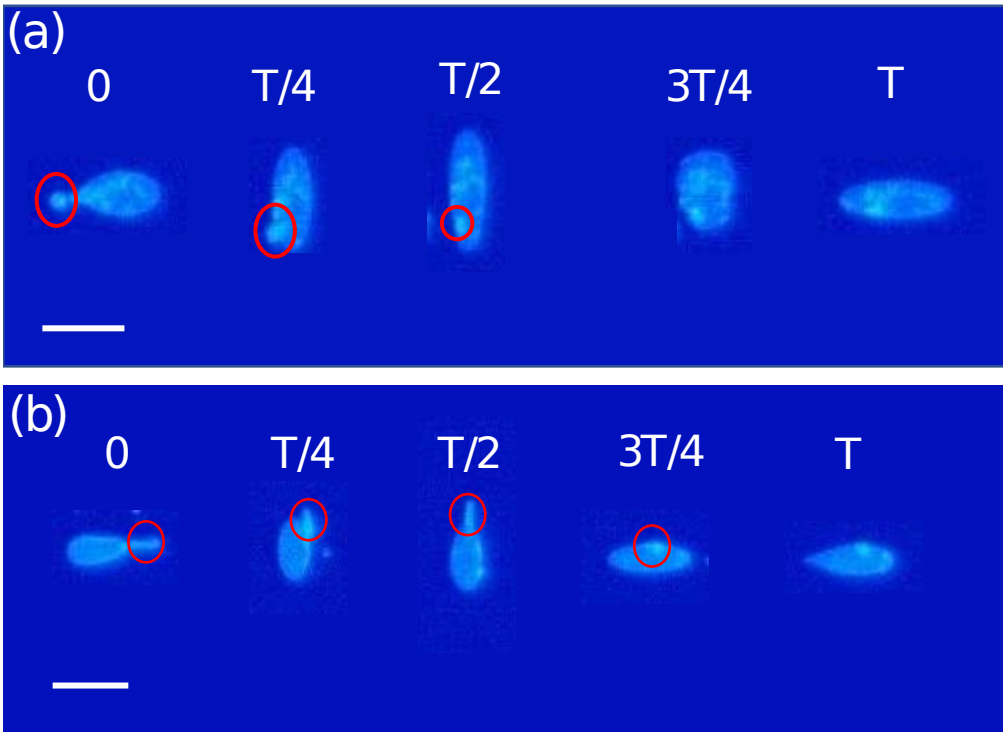

FIG. S8: Engulfment of a transient bud into the vesicle interior during LAOE cycle. (a) Ca = 260, De = 5, (b) Ca = 329, De = 144. Scale bar is 10 μm. Red circle highlights the location of bud in each snapshot.

1.4 Engulfment of a transient bud into vesicle interior in LAOE flow

Another interesting feature of complex vesicle dynamics in LAOE flow is shown in Fig. S8. As shown in Fig. S8, a vesicle with exterior buds is exposed to a full LAOE cycle deformation. Interestingly, we observed that the vesicle membrane folds in a way to engulf the bud into the vesicle interior during the flow cycle. After the bud is engulfed into the vesicle interior, we exposed the vesicle to several cycle deformations but the bud remains in the interior.

2 Theoretical Results: Vesicle in planar flow

2.1 Quasispherical vesicle

We discuss the analytical results for a vesicle in a planar extensional flow. These results assume the vesicle is quasi-spherical and hence make use of spherical harmonics to determine the flow field inside and outside the vesicle Vlahovska & Gracia (2007); Turitsyn & Vergeles (2008). We place a vesicle in the linear flow field (Fig. S9):

$$E_{ij} = -\dot{\epsilon} \begin{pmatrix} 0 & 1 & 0 \\ 1 & 0 & 0 \\ 0 & 0 & 0 \end{pmatrix} \sin(2\pi\omega t^*) \tag{1}$$

where $\dot{\epsilon}$ is the amplitude of the strain rate, ω is the frequency, and t^* is the dimensional time. The vesicle has a characteristic size a defined by the radius of a sphere of the same surface area S and a characteristic size R defined by the radius of a sphere of the same volume V. The equilibrium shape of the vesicle is characterized by a small excess area Δ:

$$\Delta = S/R^2 - 4\pi, \quad a = (S/4\pi)^{1/2}, \quad \frac{R}{a} = \left(1 + \frac{\Delta}{4\pi}\right)^{-1/2}. \tag{2}$$

Therefore the reduced volume can be written as

$$\nu = \frac{V}{4\pi a^3/3} = \left(\frac{R}{a}\right)^3 = \left(1 + \frac{\Delta}{4\pi}\right)^{-3/2}. \tag{3}$$

For small excess area ($\Delta \ll 1$), the vesicle shape is parameterized by $r = (r^*/R) = (1 + u)$ where $u(\theta, \phi)$ can be expanded in series of spherical harmonics Vlahovska & Gracia (2007) and the superscript * denotes a dimensional quantity. For planar extensional flow, there are only two modes excited Vlahovska & Gracia (2007)

$$r(t^*, \theta, \phi) = 1 + f_{2,-2}(t^*)Y_{2,-2}(\theta, \phi) + f_{2,2}(t^*)Y_{2,2}(\theta, \phi), \tag{4}$$

where f_{ij} is the time-dependent amplitude and Y_{lm} are the spherical harmonics

$$Y_{lm} = \sqrt{\frac{2j+1}{4\pi}\frac{(j-m)!}{(j+m)!}}(-1)^m P_j^m(\cos(\theta))e^{im\phi}, \tag{5}$$

To examine the deformation of the vesicle, the non-dimensional half length along the extensional axis is

$$L = r(\theta = \pi/2, \phi = \pi/4) = 1 + \frac{1}{4}\sqrt{\frac{15}{2\pi}}(f_{2,2} - f_{2,-2})\mathbb{I}, \tag{6}$$

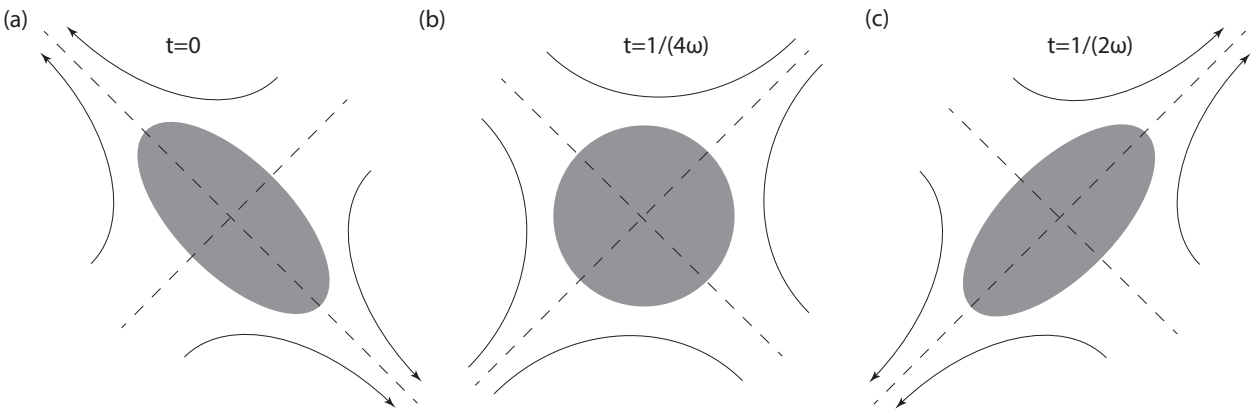

FIG. S9: The scheme illustrates moments of vesicle deformation in time-dependent extensional flow: (A) $\omega t^* = 0$, (B) $\omega t^* = 1/4$, (C) $\omega t^* = 1/2$.

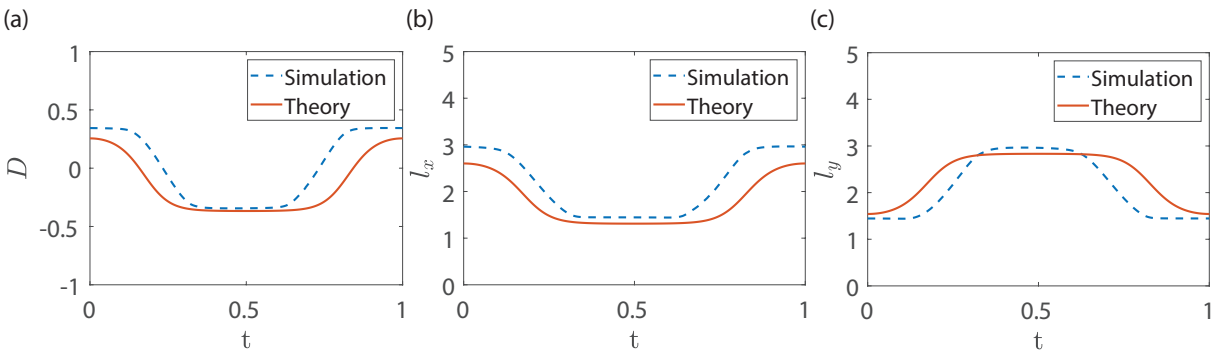

FIG. S10: The dynamic evolution of (a) D, (b) l_x & (c) l_y. In this case, Ca = 40, De = 10, $\nu = 0.9$. The viscosity ratio is $\lambda = 1$.

and the non-dimensional half length along the compression axis is

$$r(\theta = \pi/2, \phi = 3\pi/4) = 1 - \frac{1}{4}\sqrt{\frac{15}{2\pi}}(f_{2,2} - f_{2,-2})\mathbb{I}, \tag{7}$$

where $\mathbb{I}$ is the imaginary unit ($\mathbb{I}^2 = -1$). We should note that the amplitude of perturbation along the axis of the extension is written as $L - 1 = \sqrt{15/(32\pi)}(f_{2,2} - f_{2,-2})\mathbb{I}$.

It has been derived in reference Vlahovska & Gracia (2007), for an extensional flow,

$$\frac{\partial f_{jm}}{\partial t^*} = \frac{1}{(1+\lambda)}C(\lambda, j, m) + \frac{1}{(1+\lambda)Ca}\Gamma(\lambda, \sigma_o, j)f_{jm}, \tag{8}$$

where the detailed expressions of C and Γ are given in the reference Vlahovska & Gracia (2007). By going through the algebra and enforcing the incompressible membrane condition ($\dot{f}_{2,-2}f_{2,2} + \dot{f}_{2,2}f_{2,-2} = 0$), we can derive the dynamic equation in terms of L

$$\frac{\partial(L-1)}{\partial t^*} = -\frac{60}{32 + 23\lambda}\dot{\epsilon}\sin(2\pi\omega t^*)\left[1 - \left(\frac{L-1}{L_\infty - 1}\right)^2\right], \tag{9}$$

where $L_\infty = 1 + \sqrt{(15\Delta)/(32\pi)}$. We start the vesicle in its maximum stretched state $L(0) = L_0$ and watch it compress during the first half the cycle $0 < t^*\omega < \frac{1}{2}$ and stretch during the second half of the cycle $\frac{1}{2} < t^*\omega < 1$.

Let us nondimensionalize the equation by introducing variables $A = (L-1)/(L_\infty - 1)$ and $t = \omega t^*$. The dimensionless deformation coefficient A can be now solved by integrating the above equation to yield:

$$\ln\left[\frac{1+A}{1-A}\right] - \ln\left[\frac{1+A_o}{1-A_o}\right] = \frac{60}{\pi(32+23\lambda)}\frac{\mathrm{Ca}}{\mathrm{De}}\frac{1}{L_\infty - 1}\left[\cos(2\pi t) - 1\right], \tag{10}$$

where $A_o = A(t=0)$ and $\mathrm{Ca}/\mathrm{De} = \dot{\epsilon}/\omega$. From equation (10), we see that the deformation A of the vesicle is periodic, with the largest deformation occurring at $t = 0$ and the minimum deformation occurring at $t = \frac{1}{2}$. This information will allow us to determine the phase boundaries for the vesicle dynamics.

2.2 Pulsating/reorienting and reorienting/symmetrical deformation boundaries

At the pulsating/reorienting phase boundary, we expect the minimum deformation to be $A(t = 1/2) = 0$. This gives the criterion:

$$\frac{\mathrm{Ca}}{\mathrm{De}} = \frac{\pi(32+23\lambda)}{120}(L_\infty - 1)\ln\left(\frac{1+A_o}{1-A_o}\right). \tag{11}$$

At the reorienting/symmetrical phase boundary, we expect the minimum deformation to be the opposite of the initial deformation – i.e., $A(t = 1/2) = -A_0$. This yields the criterion:

$$\frac{\mathrm{Ca}}{\mathrm{De}} = \frac{\pi(32 + 23\lambda)}{60}(L_\infty - 1)\ln\left(\frac{1 + A_o}{1 - A_o}\right), \tag{12}$$

where A_o is written in the dimensional units

$$A_o = \frac{\frac{l_x^*(0)}{2a}\nu^{-1/3} - 1}{\sqrt{\frac{15}{8}}\left(\nu^{-2/3} - 1\right)^{1/2}}. \tag{13}$$

We can rewrite this expression in a more convenient form in terms of the vesicle's initial Taylor deformation parameter $D_0 = (l_x^*(0) - l_y^*(0))/(l_x^*(0) + l_y^*(0)) = L_0 - 1$. In the limit $A_o \ll 1$, $\ln\left(\frac{1+A_o}{1-A_o}\right) \approx 2A_o \approx \frac{1}{(L_\infty - 1)}\ln\left(\frac{1+D_o}{1-D_o}\right)$. Thus, we rewrite our phase boundaries as:

$$\frac{\mathrm{Ca}}{\mathrm{De}} = \frac{\pi(32 + 23\lambda)}{120}\log\left(\frac{1 + D_o}{1 - D_o}\right) \quad \text{for pulsating/reorienting phases,} \tag{14}$$

$$\frac{\mathrm{Ca}}{\mathrm{De}} = \frac{\pi(32 + 23\lambda)}{60}\log\left(\frac{1 + D_o}{1 - D_o}\right) \quad \text{for reorienting/symmetrical phases.} \tag{15}$$

Figure 8 in the manuscript shows the phase boundaries with 5% uncertainty in the initial Taylor deformation parameter D_o when the viscosity ratio is $\lambda = 1$. Fig. S10 shows the evolution of vesicle Taylor deformation parameter $D(t) = L - 1$ when $\mathrm{Ca} = 60$ and $\mathrm{De} = 10$. Lastly, Fig. S13 plots the theoretical phase boundaries for viscosity ratios of $\lambda = 0.1$ and $\lambda = 10$.

The $\lambda = 0.10$ theoretical phase boundary does not match quantitatively with the numerical simulations unlike other values of the viscosity ratio. We believe this discrepancy arises because the analytical theory is only valid for quasi-spherical vesicles, but the deformation at lower viscosity ratios appears significant. For lower viscosity ratios, we expect the theory to better reflect the simulations for reduced volumes very close to unity, where the quasi-spherical limit will be strictly valid.

3 Surface area and volume conservation

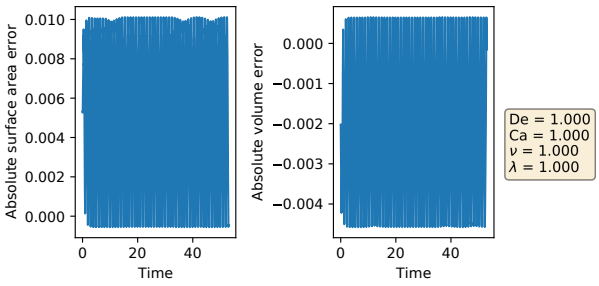

(a) Pulsating regime

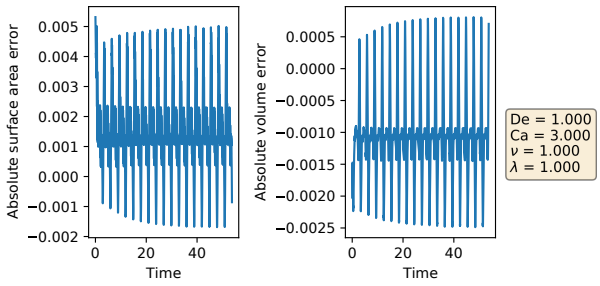

(b) Reorienting regime

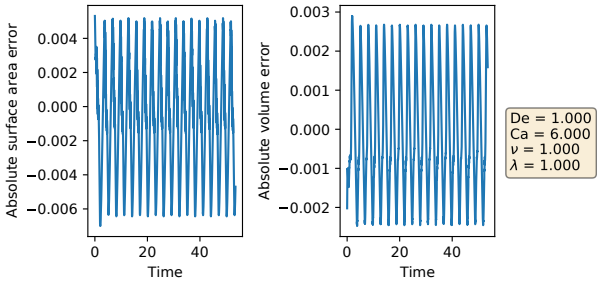

(c) Symmetrical regime

FIG. S11: Surface area and volume conservation for simulations in the pulsating, reorienting, and symmetrical regimes. Absolute errors are shown. We use an equivalent length of 1 in the simulations, so the target surface area is 4π and the target volume is $\frac{4}{3}\pi$.

4 Element size convergence study for deformation parameter

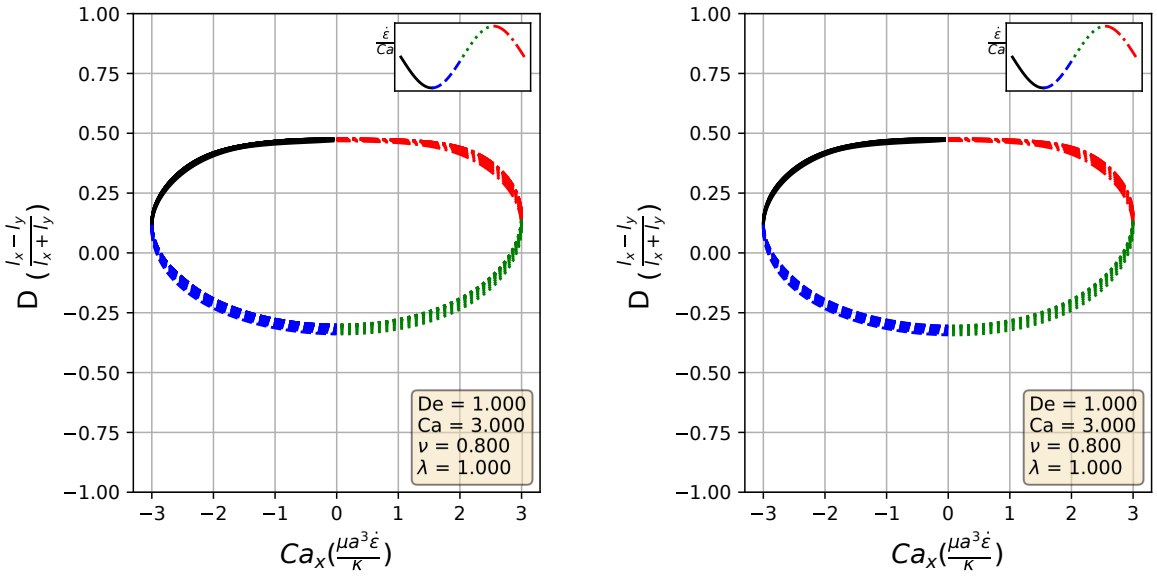

(a) 1280 element simulation

(b) 9680 element simulation

FIG. S12: Lissajous type curves for the deformation parameter over several flow cycles. No significant differences were observed for mesh sizes from 720 elements to 9680 elements.

5 Phase diagrams for different viscosity ratios

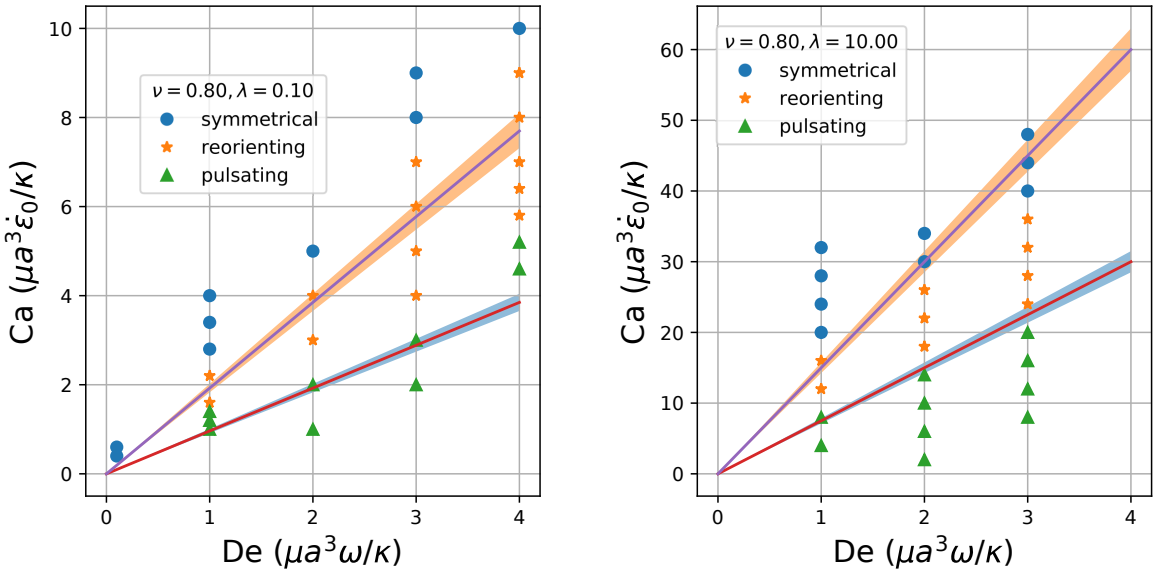

(a) (b)

FIG. S13: Phase diagrams for other viscosity ratios. 5% error in the slope included in the analytical lines for numerical calculation of D_o

6 Supplementary Movies

Movie 1 : Side-by-side comparison of simulation and experimental video of a quasi-spherical vesicle of reduced volume $\nu = 0.88$. The vesicle is deformed in the pulsating regime at $Ca = 10.9$, $De = 18.2$, and $\lambda = 1.00$. Experimental movie speed is 2X.

Movie 2 : Side-by-side comparison of simulation and experimental video of a quasi-spherical vesicle of reduced volume $\nu = 0.88$. The vesicle is deformed in the reorienting regime at $Ca = 10.9$, $De = 4.5$, and $\lambda = 1.00$. Experimental movie speed is 2X.

Movie 3 : Side-by-side comparison of simulation and experimental video of a quasi-spherical vesicle of reduced volume $\nu = 0.88$. The vesicle is deformed in the symmetrical regime at $Ca = 10.9$, $De = 3$, and $\lambda = 1.00$. Experimental movie speed is 2X.

Movie 4 : Side-by-side comparison of simulation and experimental video of a tubular vesicle of reduced volume $\nu = 0.64$. Experimental uncertainty of ± 0.02 for reduced volume measurement. The vesicle is deformed at $Ca = 21.3$, $De = 17.7$, and $\lambda = 1.00$ and displays pulsating like dynamics with wrinkling. Buckling of vesicle membrane is clearly visible during the compression phase of the flow. Experimental movie speed is 2X.

Movie 5 : Side-by-side comparison of simulation and experimental video of a tubular vesicle of reduced volume $\nu = 0.64$. Experimental uncertainty of ± 0.02 for reduced volume measurement. The vesicle is deformed at $Ca = 21.3$, $De = 8.9$, and $\lambda = 1.00$ with reorienting/pulsating like dynamics with wrinkling. In the experiments, change in 2D shape of the vesicle can be seen over repeated LAOE cycles. Experimental movie speed is 2X.

Movie 6 : Side-by-side comparison of simulation and experimental video of a tubular vesicle of reduced volume $\nu = 0.64$. Experimental uncertainty of ± 0.02 for reduced volume measurement. The vesicle is deformed at $Ca = 21.3$, $De = 4.7$, and $\lambda = 1.00$ and displays symmetrical/reorienting like dynamics. In the experiments, change in 2D shape of the vesicle can be seen over repeated LAOE cycles. Experimental movie speed is 2X.

Movie 7 : A quasi-spherical vesicle simulation of reduced volume $\nu = 0.80$ shown in the pulsating, reorienting, and symmetrical regimes at Ca $= [2.0, 3.0, 4.0]$, De $= 1.00$, and $\lambda = 1.00$.

Movie 8 : A prolate vesicle that starts aligned with the z-axis of $\nu = 0.80$, Ca $= 3.00$, De $= 1.00$, and $\lambda = 1.00$. Deforms symmetrically.

Movie 9 : A prolate vesicle that starts aligned 70 degrees rotated in the y-axis from the original x-axis orientation, such that is it is 30 degrees offset from the z-axis. Dynamics observed are equivalent to those seen in the symmetrical regime at other starting orientations, parameters of $\nu = 0.80$, Ca $= 6.00$, De $= 1.00$, and $\lambda = 1.00$.

Movie 10 : A prolate vesicle that starts aligned 70 degrees rotated in the y-axis from the original x-axis orientation, such that is it is 30 degrees offset from the z-axis. Maintains off flow axis orientation, parameters of $\nu = 0.80$, Ca $= 3.00$, De $= 1.00$, and $\lambda = 1.00$.

References

Turitsyn, KS & Vergeles, SS 2008 Wrinkling of vesicles during transient dynamics in elongational flow. *Physical review letters* **100** (2), 028103.

Vlahovska, Petia M & Gracia, Ruben Serral 2007 Dynamics of a viscous vesicle in linear flows. *Physical Review E* **75** (1), 016313.